

The front condition for gravity currents

By **B. M. MARINO**¹, **L. P. THOMAS**¹
AND **P. F. LINDEN**²

¹Instituto de Física Arroyo Seco, Facultad de Ciencias Exactas, Universidad Nacional del Centro de la Pcia. de Buenos Aires, Pinto 399, B7000GHG Tandil, Argentina

²Department of Mechanical and Aerospace Engineering, University of California, San Diego, 9500 Gilman Drive, La Jolla, CA 92093-0411, USA

(Received 11 May 2004 and in revised form 8 February 2005)

Self-similar plane solutions for the inertial stage of gravity currents are related to the initial parameters and a coefficient that is determined by the boundary condition at the front. Different relations have been proposed for the boundary condition in terms of a Froude number at the front, none of which have a sound theoretical or experimental basis. This paper focuses on considerations of the appropriate Froude number based on results of lock-exchange experiments in which extended inertial gravity currents are generated in a rectangular cross-section channel. We use ‘top-hat’ vertical density profiles of the currents to obtain an ‘equivalent’ depth, defined by profiles having the same buoyancy at every position as the real profiles. As in previous work, our experimental results show that in the initial constant-velocity phase the Froude number can be defined in terms of the lock depth. However, as the current enters the similarity phase when the initial release conditions are no longer relevant, we find that the Froude number is more appropriately defined in terms of the maximum height of the head. Strictly speaking, the self-similar solution to the shallow-water equations requires a front condition that uses the height at the rear of the head. We find that this rear Froude number is not constant and is a function of the head Reynolds number over the range 400–4500.

1. Introduction

Gravity currents occur when fluid of one density propagates along a horizontal boundary into fluid of a different density. There are many examples of gravity currents, both naturally occurring and man made, and a comprehensive set of examples can be found in Simpson (1997).

Gravity currents have been studied extensively in laboratory experiments since the 1950s, and measurements made of their speed of propagation. The usual form of these experiments is to place a vertical barrier in a channel and place, say, fresh water on one side and salt water on the other side. When the barrier is removed the salt water flows along the bottom of the channel underneath the fresh water in one direction, while the fresh water flows along the surface above the salt water in the other direction. This is known as a full-depth lock-exchange flow. The speed of the two currents can be measured and related to the densities of the fresh and salt water, the depth of the channel and the viscosity of the fluids.

A discussion of some of the history of these experiments can be found in Shin, Dalziel & Linden (2004) and will not be repeated here. The salient facts are that, after an initial acceleration from rest, the speed of the front of the current is observed

to be constant (within experimental error) for a period and then to decelerate. This behaviour can be deduced from dimensional analysis. Let U denote the speed of the front, and suppose that the densities of the two fluids are ρ_1 and $\rho_2 > \rho_1$. In a channel of depth H , a velocity independent of time must, if viscous forces are ignored for the moment, be given by

$$U = F\sqrt{g'_0 H}, \quad (1.1)$$

where $g'_0 = g(\rho_2 - \rho_1)/\rho_2$ is the reduced gravity and F is a dimensionless constant†. Measurements of F for full-depth lock exchanges were made by Keulegan (1958) and Barr (1967) and found to vary between 0.45 and 0.5, for sufficiently high Reynolds numbers.

In many experiments, the barrier is placed near one end of the tank, in order to give a long length of channel for measurements of the current to be made. Suppose that the salt water is placed in this small 'lock' and that the rest of the tank is filled with 'ambient' fresh water. The flow initially proceeds as above, but now the fresh water entering the small lock displaces all the salt water well before the salt current has reached the other end of the channel. In this case, the finite length L_0 of the lock becomes a parameter that must be considered. Alternatively, we can use the finite volume of salt water as the parameter, while taking the depth of the ambient fresh water to be effectively infinite since the current depth decreases when it propagates sufficiently far from the lock. Hence, the speed of the current now depends on the total mass (per unit width of the channel), which can be expressed by the initial buoyancy per unit width $B_0 = g'_0 H L_0$. Under these circumstances, dimensional analysis implies that

$$U = c B_0^{1/3} t^{-1/3}, \quad (1.2)$$

where c is a dimensionless constant, and the current decelerates with time, or distance along the channel. Values of c have been measured by Houtl (1972) and Huppert & Simpson (1980), and their data suggest $c \approx 1.0$. The initial constant-velocity phase given by (1.1) and the subsequent, so-called, similarity phase given by (1.2), represent force balances between buoyancy and inertia. As the current continues to decelerate and the Reynolds number decreases, viscous effects may become important and a further dependence of velocity on time occurs. When the buoyancy forces are balanced by viscous forces, the speed $U \sim t^{-4/5}$.

Among others, Fay (1969), Fannelop & Waldman (1972), Houtl (1972), Huppert & Simpson (1980) and Rottman & Simpson (1983) established the theoretical basis of the asymptotic self-similar flows originated by instantaneous releases when the buoyancy force driving the current is balanced by inertia. This assumption leads to the result that the length (or the radius in an axisymmetric flow) increases as $t^{2/(3+n)}$, where $n=0$ and $n=1$ for plane and axisymmetric flows, respectively. In particular, Fannelop & Waldman (1972) and Houtl (1972) showed that (1.2) results from a similarity solution of the shallow-water equations, and so the relationship is valid only after a long time has elapsed since release. Grundy & Rottman (1985) confirmed mathematically that these similarity solutions are the large-time limits of a class of initial-value problems associated with the shallow-water equations in which mixing is neglected and the front region is treated as an abrupt boundary condition. Gratton & Vigo (1994) further investigated all possible self-similar solutions for inertial gravity

† Strictly speaking, F is a dimensionless function of the density ratio $\gamma = \rho_1/\rho_2$, but we are concerned with Boussinesq currents where $\gamma \approx 1$, and so γ does not enter as a separate dimensionless parameter.

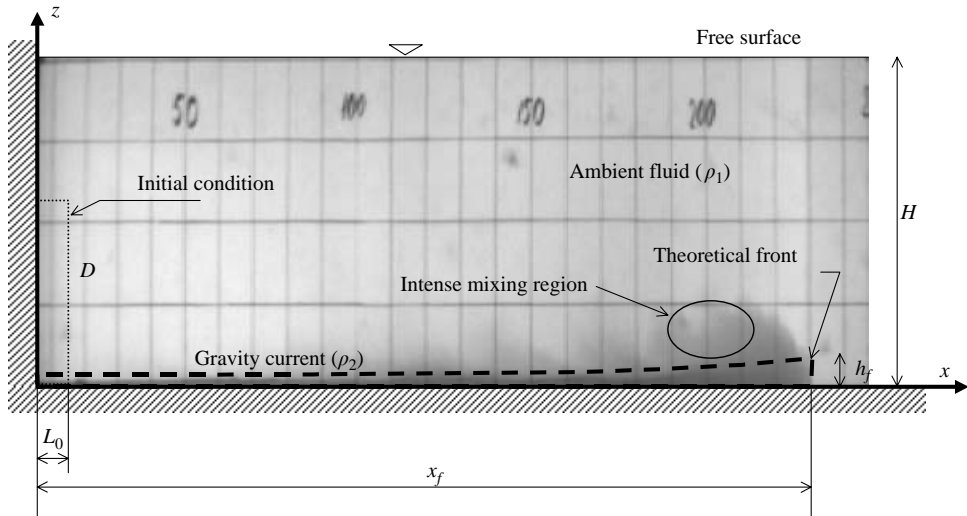


FIGURE 1. Lock-release gravity current as obtained in the laboratory. The dashed line indicates the usual approach considered in analytical treatments.

currents by analysing the mathematical properties of a phase plane, and showed that a family of solutions exists for each value of a dimensionless front velocity.

Based on the measurements of the constant-velocity phase, the front is represented in the shallow-water framework by a condition that relates the front speed u_f to the local buoyancy force $g'_f h_f$, where the subscript f denotes local values at the front. This takes the form of a constant local Froude number F_f , obtained by re-arranging (1.1) and applying it at the front so that

$$F_f = \frac{u_f}{\sqrt{g'_f h_f}}. \quad (1.3)$$

This relation is especially pertinent in applications to natural flows. These do not, in general, occur in channels of finite depth, or from finite releases of known buoyancy, so the speeds given by (1.1) and (1.2) are not very useful. Theory does not help much either. The only theories that predict the front speed are for the constant-velocity phase (Benjamin 1968; Shin *et al.* 2004). These theories both predict the Froude number in terms of the ‘fractional depth’ of the current – i.e. the depth of the current as a fraction of the total depth of the flow. In the often relevant limit where the ambient fluid is much deeper than the current, these two theories give values that differ by 40 %. Laboratory experiments such as those reported by Huppert & Simpson (1980) are also for the constant-velocity phase. We discuss these earlier results in more detail in §2.

It is also not obvious that a front condition appropriate to the constant-velocity phase should be valid in the similarity phase. In the former, the current propagates as though the dense fluid is supplied continuously from the rear at a constant rate, while the similarity phase is a direct consequence of the fact that the volume of dense fluid is finite. Rottman & Simpson (1983) show that the transition to the similarity phase is initiated by a finite-amplitude disturbance that is reflected at the rear wall of the lock and propagates to the front of the current.

A major difficulty comes from the complexity of the flow in a real gravity current. Figure 1 illustrates a gravity current as treated by theory (dashed line contour), and

as seen in laboratory experiments and in many natural flows. The front of the current, a region of mixing and unsteady motions, must be represented by some equivalent depth and density.

Most previous studies have used the front position $x_f(t)$, a parameter that is easy to measure, to test their theories. On the other hand, the measurement of the appropriate height of the current to calculate the Froude number is difficult because real currents exhibit a deeper head than the following fluid, and mixing between dense and ambient fluids prevents the determination of a well-defined boundary. The height profile of the current is irregular and unsteady.

This paper concentrates on the determination of the front condition for the similarity phase by comparing the theoretical self-similar solutions with the results provided by lock-exchange experiments in which inertial gravity currents are generated in a rectangular cross-section channel starting from a small-length lock. Our goal is to display the interrelation among the front position evolution, the Froude number at the front and the height profiles based on the measurements of the density distributions. By using measured vertical density profiles, the buoyancy and the equivalent height of the current can be determined objectively and unambiguously.

In §2, the theoretical framework is discussed further, and a relationship associating the flow at the front with the Froude number depending on the instantaneous fractional depth $\phi(t) = h_f(t)/H$ at the front is suggested. Section 3 contains a description of the experiments and techniques used to find the ‘equivalent current height’ that is calculated from the local buoyancy and, as it is unaffected by mixing, becomes the appropriate parameter to use in comparisons. The experimental results are presented in §4 and discussed in §5. The conclusions are given in §6.

2. Theoretical framework

2.1. Self-similar solution for a plane gravity current

We are concerned with planar self-similar solutions for gravity currents in the shallow-water approximation. The currents are generated by the instantaneous release of a fixed volume of a fluid of density ρ_2 into another fluid of lower density ρ_1 over a solid horizontal surface.

Shallow-water theory (Landau & Lifshitz 1987) is based on the fact that the depth of the current is small compared with the characteristic horizontal scales of the flow. Then the vertical accelerations of the fluid are small compared to gravity. Thus the pressure variation is hydrostatic and, for a planar flow, the fluid motion depends on the horizontal coordinate x and time t , with the horizontal velocity $u(x, t)$ constant throughout the current depth $h(x, t)$.

Self-similar solutions to the shallow-water equations for gravity currents are obtained by neglecting mixing and treating the front region as an abrupt boundary with some specified front condition (Grundy & Rottman 1985; Gratton & Vigo 1994). These solutions represent the intermediate asymptotic solutions in which most of the parameters and features describing the initial physical situation have become irrelevant, even though some features of the initial-value problem remain (Barenblatt 1996; Gratton & Vigo 1994).

For the case of the release of a volume concentrated in $x=0$ at $t=0$ into an infinitely deep ambient fluid, the self-similar theory gives the front position x_f as a function of time as

$$x_f = \xi(g'_0 A_0)^{1/3} t^{2/3}, \quad (2.1)$$

where ξ is a dimensionless constant. The self-similar solution, in agreement with the result of the dimensional analysis discussed in §1, depends only on the initial buoyancy (per unit width) $B_0 = g'_0 A_0$, where $A_0 = L_0 D$ is the area (volume per unit width) occupied initially by the dense fluid. Conservation of mass implies that B_0 is a constant throughout the motion of the current, irrespective of mixing between the current and the ambient fluid. We restrict attention to Boussinesq currents with $\rho_2 - \rho_1 \ll \rho_2$. Equation (2.1) describes the asymptotic behaviour for $t \gg t_c = L_0/u_0$ where t_c is the time taken for a wave propagating with speed $u_0 = \sqrt{g'_0 D}$ to travel the length L_0 of the lock. To facilitate the comparison with the experimental results, it is convenient to express (2.1) in dimensionless form as

$$\frac{x_f}{L_0} = \xi \left(\frac{t}{t_c} \right)^{2/3}. \quad (2.2)$$

Note that such a solution does not depend on the particular values of L_0 and t_c . Differentiating (2.2) with respect to time, the velocity of the front is given by

$$\frac{u_f}{u_0} = \frac{dx_f}{dt} \frac{t_c}{L_0} = \frac{2}{3} \xi \left(\frac{t_c}{t} \right)^{1/3} = \frac{2}{3} \xi^{3/2} \left(\frac{L_0}{x_f} \right)^{1/2}. \quad (2.3)$$

As Grundy & Rottman (1985) and Gratton & Vigo (1994) reported, the height profile for a self-similar plane gravity current is

$$\frac{h(x/x_f)}{h_f} = \frac{x_f}{x} \left[\frac{F_f^2}{4} + \left(1 - \frac{F_f^2}{4} \right) \left(\frac{x}{x_f} \right)^2 \right], \quad (2.4)$$

where

$$h_f = \left(\frac{12}{12 - 2F_f^2} \right) \left(\frac{A_0}{x_f} \right) \quad (2.5)$$

is the current height, and F_f is given by (1.3).

From (2.3), (2.5) and (1.3) it is found that ξ is related to the Froude number by

$$\xi^3 = \frac{27F_f^2}{12 - 2F_f^2}. \quad (2.6)$$

As demonstrated by Gratton & Vigo (1994), a self-similar solution exists for any value of $F_f < \sqrt{6}$. Therefore, the Froude number at the front for any particular situation must be estimated using an additional condition.

As the current propagates, it reduces its velocity and height and, as the Reynolds number decreases, eventually enters the viscous phase. Huppert (1982) showed that in this buoyancy-viscous phase the front position is described by the power law

$$x_f = \zeta \left(\frac{B_0 A_0^2}{3\nu} \right)^{1/5} t^{1/5}, \quad (2.7)$$

where ν is the kinematic viscosity and $\zeta = 1.411 \dots$ is completely defined by theory. Note that (2.7) shows that the corresponding front velocity depends only upon B_0 and ν . In terms of the scale u_0 , as needed for comparing the theoretical estimates with the experimental results introduced in §4, the non-dimensional velocity is

$$\frac{u_f}{u_0} = \frac{dx_f}{dt} \frac{t_c}{L_0} = \frac{\zeta^5}{5} \left(\frac{1}{L_0^4 u_0} \right) \left(\frac{B_0 A_0^2}{3\nu} \right) \left(\frac{L_0}{x_f} \right)^4, \quad (2.8)$$

which gives a different curve for each set of initial parameters when the spatial (L_0) and temporal (t_c) characteristic scales are used. Note also that the front velocity (2.8) decreases more rapidly than in the buoyancy-inertial self-similar regime (2.3) as x_f increases. In this asymptotic viscous phase the height profile is given by (Marino *et al.* 1996)

$$\frac{h}{h_0} = \left[1 - \left(\frac{x}{x_f} \right)^2 \right]^{1/3}. \quad (2.9)$$

2.2. Froude number at the front for lock-exchange currents

In contrast with the above analysis where the depth of the ambient fluid is assumed to be infinite, experiments always have a finite depth H of ambient fluid. For lock-exchange gravity currents at the constant-velocity phase, different relationships for the Froude number at the front have been proposed. Benjamin (1968) applied hydraulic theory to the planar flow of an incompressible fluid in a channel in terms of an ‘air cavity flow’ displacing the fluid beneath it.

Figure 2(a) illustrates this flow in the frame of reference that moves with the front of the cavity; the original nomenclature has been changed to facilitate comparison with the relationships obtained by other authors. Benjamin (1968) found that the Froude number is given by

$$F_B = \frac{u_2}{\sqrt{g'_0 h_B}} = \left[\frac{(1-\phi)(2-\phi)}{1+\phi} \right]^{1/2}, \quad (2.10)$$

where $u_f = u_2$, h_B and $\phi = h_B/H$ are the fluid velocity upstream (i.e. the front velocity in the laboratory frame), the cavity height and the fractional depth, respectively. For a cavity, $g'_0 = g$, but Benjamin showed that his result applies to the Boussinesq case also.

Figure 2(b) illustrates the configuration studied experimentally by Huppert & Simpson (1980). They observed that initially the current travels at a constant speed and the Froude number F_{HS} was determined using the height of the current h_{HS} ‘just behind the head’ and found to fit the empirical relation

$$F_{HS} = \frac{u_2}{\sqrt{g'_0 h_{HS}}} = \begin{cases} 1.19 & (\phi \leq 0.075), \\ \frac{1}{2}\phi^{-1/3} & (\phi > 0.075), \end{cases} \quad (2.11)$$

where $\phi = h_{HS}/H$.

In their solution of the shallow-water equations in a two-layer fluid, Rottman & Simpson (1983) proposed an empirical front condition by defining the Froude number

$$F_{RS} = \frac{u_f}{\sqrt{g'_0 h_{RS}}} = \left[\frac{\beta^2 (1-\phi)(2-\phi)}{2(1+\phi)} \right]^{1/2}, \quad (2.12)$$

where β is a dimensionless constant to be determined by experiments, h_{RS} is a theoretically defined height at the front and $\phi = h_{RS}/H$. When $\beta^2 = 2$, (2.12) gives the relationship for the front speed derived by Benjamin (2.10).

Shin *et al.* (2004) have presented a new theory and experiments on gravity currents in the constant-velocity phase produced by lock-exchange. They suggest that the energy dissipation inside the flow is unimportant for high Reynolds numbers, and that long waves may transfer momentum and energy from one side of the lock to the other, modifying the front velocity. Based on energy conservation in the control volume depicted with a dashed line in figure 2(c), the authors obtained the following

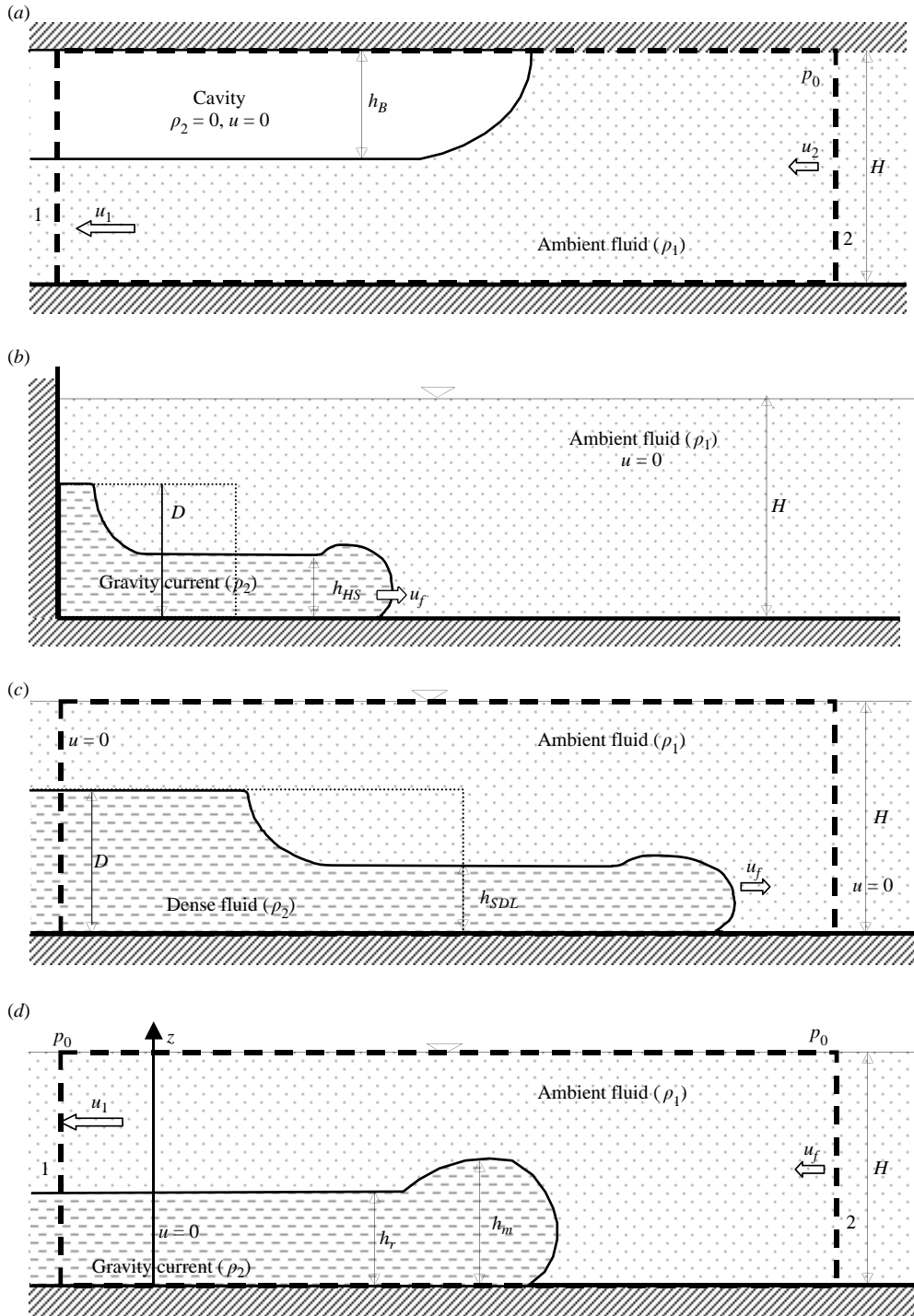


FIGURE 2. Sketches used to define the Froude number at the current front according to (a) Benjamin (1968), (b) Huppert & Simpson (1980), (c) Shin *et al.* (2004) and (d) the analysis presented in this work.

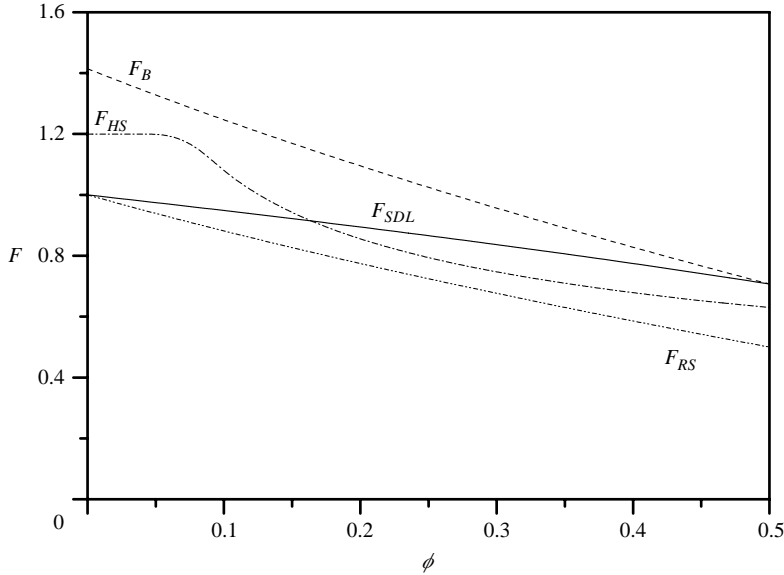


FIGURE 3. Froude number F as a function of the fractional depth ϕ suggested by different theories for a constant-velocity gravity current. The curve F_{RS} , given by (2.12), is represented for $\beta^2 = 1$ as suggested by Rottman & Simpson (1983).

relationship for the Froude number

$$F_{SDL} = \frac{u_f}{\sqrt{g'_0 h_{SDL}}} = (1 - \phi)^{1/2}, \quad (2.13)$$

where $\phi = h_{SDL}/H$, and h_{SDL} is the depth of the current measured at the original lock position.

Figure 3 presents a comparison between the Froude number at the front as a function of ϕ calculated from the relations (2.10) to (2.13). Benjamin (1968) and Shin *et al.* (2004) demonstrated that in addition to mass and momentum conservation, energy is also conserved for $\phi = 0.5$, and the two theories give the same value $1/\sqrt{2}$ for this particular value of ϕ . However, in the rest of the interval the curves do not coincide with each other. Huppert & Simpson (1980) and Rottman & Simpson (1983) do not give the same values at $\phi = 0.5$. (Note that values of $\phi > 0.5$ are believed to be unrealizable in lock-exchange since they require input of external energy into the flow – see Benjamin 1968; Shin *et al.* 2004).

These different formulae for F give very different predictions for the limit of infinitely deep ambient fluids ($\phi \rightarrow 0$). In particular, Benjamin (1968) predicts $F_B = \sqrt{2}$, Shin *et al.* (2004) and Rottman & Simpson (1983) have the limit of $F_{SDL} = 1$, and the empirical relationship of Huppert & Simpson (1980) gives the intermediate value $F_{HS} = 1.19$. These values, in turn, give values of the dimensionless similarity coefficient in (2.6) of $\xi_B \simeq 1.89$, $\xi_{HS} \simeq 1.62$ and $\xi_{SDL} \simeq 1.39$. The values of ξ determined from experiments by Hoult (1972) and Huppert & Simpson (1980) are 1.6 and 1.5, respectively, as discussed in §1. Note, however, that these theoretical values of F are strictly only valid for the constant-velocity phase. There is no guarantee that they are appropriate for the decelerating similarity phase.

Run	Symbol	D (cm)	ϕ_0	g'_0 (cm s $^{-2}$)	t_c (s)	$u_0 D/\nu$
1	□	10	1	0.944	3.255	2790
2	⊠	10	1	4.89	1.430	6360
3	▣	10	1	8.99	1.055	8620
4	▢	10	1	29.22	0.585	15 500
5	□	10	1	98.0	0.320	28 500
6	⊖	20	1	9.80	0.714	25 500
7	⊗	20	1	5.66	0.940	19 300
8	○	20	1	98.0	0.226	80 500
9	△	30	1	8.50	0.626	43 500
10	◇	40	1	10.50	0.488	74 500
11	◇	40	1	98.0	0.160	228 000
12	△	28	1	98.0	0.191	133 000
13	*	27	0.675	9.80	0.615	39 900
14	+	20	0.5	8.80	0.754	24 100
15	—	10	0.25	8.80	1.066	8530
16		16	0.4	9.80	0.799	18 200
17	■	22	0.55	27.93	0.403	49 600
18	●	24.5	0.61	29.40	0.373	59 800
19	▼	21.5	0.54	8.80	0.727	26 900

TABLE 1. Main parameters of the experiments.

3. Experiments

Gravity currents were generated in a horizontal and rectangular cross-section channel 3.00 m long, 0.20 m wide and 0.60 m deep with transparent Perspex sidewalls. As illustrated in figure 1, the dense fluid (salt water) was initially contained in a lock with a vertical gate located at a distance L_0 from one endwall of the tank. The lock and the rest of the channel were filled up to a height D with salt water and fresh water, respectively. A known quantity of dye was mixed in the dense water contained in the lock to provide flow visualization. Then fresh water was carefully added on both sides of the lock gate to a total depth H , creating in the lock a clearly defined horizontal density interface between the salt water and fresh water. The experiment starts when the gate is removed, leaving the dense fluid to flow along the bottom of the tank.

As our study is concerned with the evolution of extended gravity currents ($x_f \gg L_0$) in order to focus on the self-similar regime, L_0 is taken as small as possible. In all cases, the lock length $L_0 = 10$ cm, and the lock aspect ratio D/L_0 varied from 1 to 4. Experiments were carried out varying both the initial reduced gravity g'_0 and the initial depth D of the dense fluid so that the initial fractional depth $\phi_0 = D/H$ is in the range $0.25 \leq \phi_0 \leq 1$. We refer to experiments with $\phi_0 = 1$ as full-depth releases and those with $\phi_0 < 1$ as partial-depth releases. Table 1 gives the parameters of the experiments. The kinematic viscosity of the salt solution is taken as $\nu = 1.1 \times 10^{-6} \text{ m}^2 \text{ s}^{-1}$.

Fluorescent strip lights and a light-diffusing screen on one side of the tank provided a back-lighting with a spatial variation of intensity of less than 7%. A COHU 4910 CCD camera was placed at a fixed position (6.00 m) from the other side of the tank and the images were digitized in real time using the software *DigImage* (Dalziel 1993, 1995) and stored in a PC. The variation of the back-lighting intensity is corrected to less than 1% by standard image-processing techniques. Then the width-averaged dye

concentration present in the salt water is measured, based on the light attenuation of the back-lighting, from which the cross-current average density may be inferred. By integrating the density distribution, the salt-water mass was also calculated for different times and was found to remain constant within a 2% error.

In order to determine the local Froude number, it is necessary to measure the height of the current. Since the hydrostatic pressure determines the dynamics of the flow in the shallow-water approximation, an equivalent height \bar{h} for each x -position is calculated, integrating vertically the instantaneous two-dimensional density distribution using

$$\bar{h}(x, t) = \int_0^H \frac{\rho(x, z, t) - \rho_1}{\rho_2 - \rho_1} dz. \quad (3.1)$$

Since ρ_2 is the original density of the fluid in the lock, in the absence of mixing, \bar{h} would correspond to the top of the current. In the presence of mixing, the equivalent height may be thought of as the height of the current in which the density is represented as a ‘top hat’ profile with

$$\rho(z) = \begin{cases} \rho_2 & (0 \leq z \leq \bar{h}), \\ \rho_1 & (z > \bar{h}). \end{cases} \quad (3.2)$$

The definition (3.1) provides an objective measure of the depth of the current. In particular, hydrostatic pressure excess at the bottom of the current is given by $g'_0 \bar{h}$ even in the presence of mixing, and this product can be used unambiguously in the definition of the Froude number (see also Shin *et al.* 2004).

From each equivalent height profile, the front position is chosen as the minimum value of x for which the equivalent height of the current is zero. The maximum equivalent height \bar{h}_m of the head is determined by taking the maximum value of \bar{h} in each frame. In most cases, the maximum value was constant for several pixels and was determined unambiguously. The equivalent height \bar{h}_r (located at the position x_r) is the value taken at the rear of the head after a change in the spatial derivative of the height profile (see figure 2*d*). The location of the derivative change is somewhat subjective and where there is significant uncertainty, the values of \bar{h}_r are discarded. These measurements of the density distribution generate an uncertainty in the height determination that is less than the pixel size, for the typical heights measured in this work. Thus the uncertainty of height values is taken as the minimum vertical scale division (2 mm) in the digitized images.

We estimate that x_f is determined with an error less than 0.6 cm and the uncertainty in the density measurement is less than 1%.

4. Results

4.1. Qualitative features and front speeds

4.1.1. Full-depth releases

Figure 4 shows eight images after processing and the associated equivalent height profiles for a typical full-depth release ($\phi_0 = 1$). The current is characterized by a raised head and a shallower following current. Typically, the length of the head is greater than its height (note that the images and the graph have an exaggerated vertical scale). Both the irregularity of the contour in the top of the head due to shear instabilities (Simpson 1997) and the vertical density distribution complicate the height estimates when they are taken directly from the individual images, as has been done

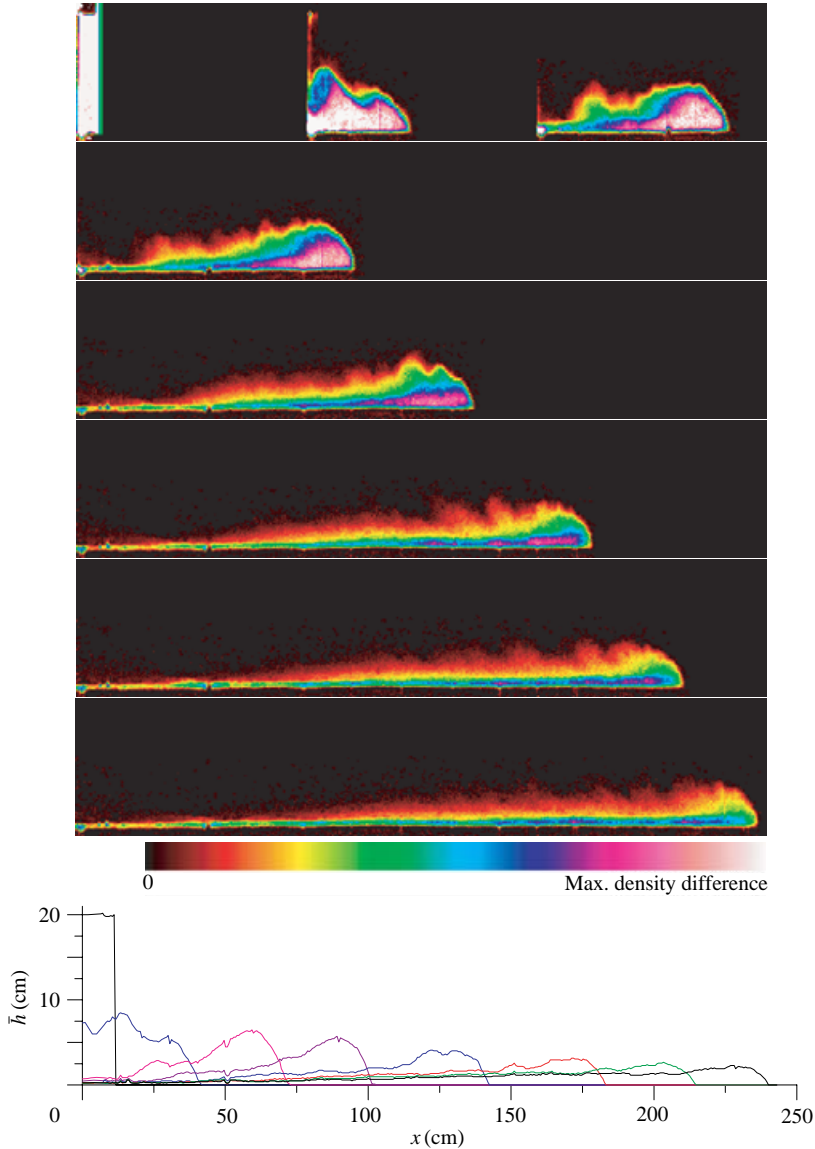


FIGURE 4. Images in false colour for fluid density and the corresponding equivalent depth profiles for run 8 with fractional depth $\phi_0 = 1$ (see table 1), for $t = 0, 1.48, 3.08, 4.68, 7.08, 9.80, 12.20$ and 14.44 s.

in most of the earlier studies. However, equivalent height profiles may be determined without ambiguity, as can be seen in figure 4.

The dimensionless front positions are plotted against the dimensionless time for runs 1–12, in which the initial fractional depth $\phi_0 = 1$, in figure 5(a). The front positions are scaled with L_0 and time with the characteristic time t_c . The dashed line on this log–log plot has slope 1 and corresponds to the theoretical curve (1.1) for the constant-velocity phase. This line is a best fit to the data and gives a value of $F = 0.47 \pm 0.02$, consistent with the previous measurements quoted in §1. At about

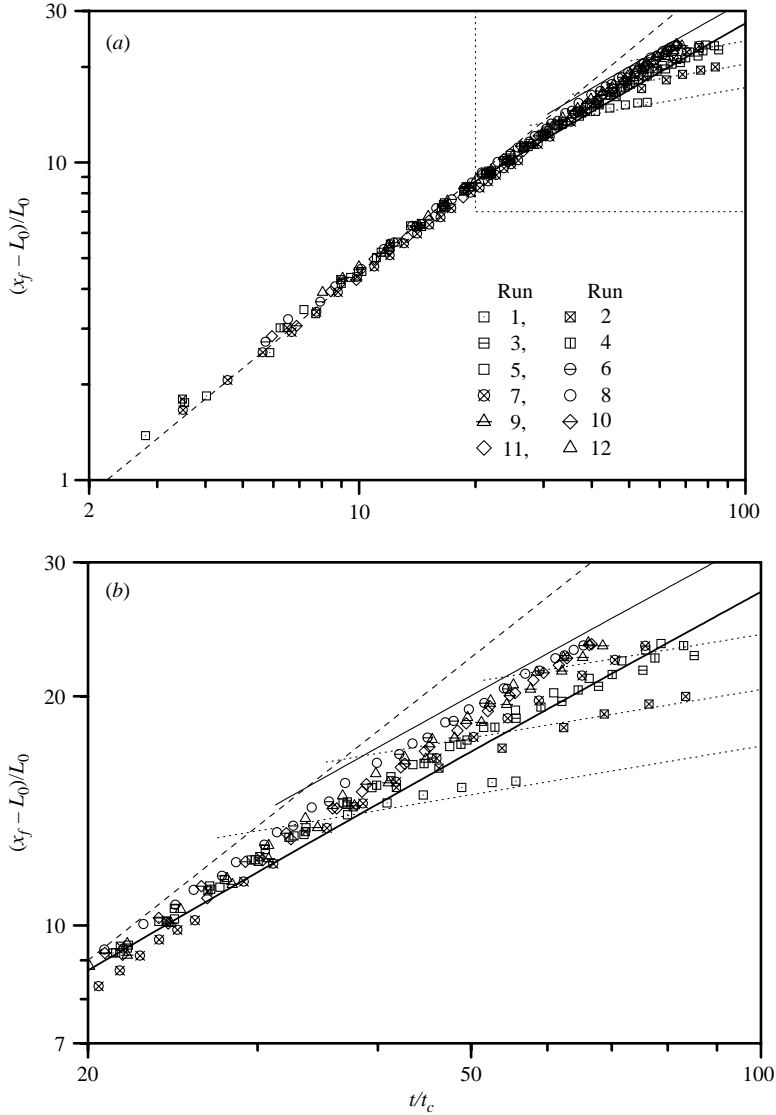


FIGURE 5. Dimensionless front position as a function of dimensionless time for full-depth releases ($\phi_0 = 1$). The theoretical front evolution for the constant-velocity phase, the inertial and the viscous self-similar regimes are indicated by the dashed, solid and dotted lines, respectively. (b) is a zoom of the region marked with a dotted line in (a). The symbols for the different runs given here and in figure 8 are used consistently throughout this paper.

8–10 lock lengths $(x_f - L_0)/L_0$, the front position is no longer a linear function of time and the currents begin to decelerate. This observation is consistent with the previous experiments of Rottman & Simpson (1983).

Also indicated in figure 5(a), and shown with more detail in the close up, figure 5(b), are the curves describing the theoretical similarity phase with values of $\xi = 1.3$ and 1.6 that limit the span of the data. As the vertical axis represents $x_f/L_0 - 1$, the self-similar curves eventually become linear with the slope $2/3$ given by (2.2) for $x_f \gg L_0$ in this log-log plot.

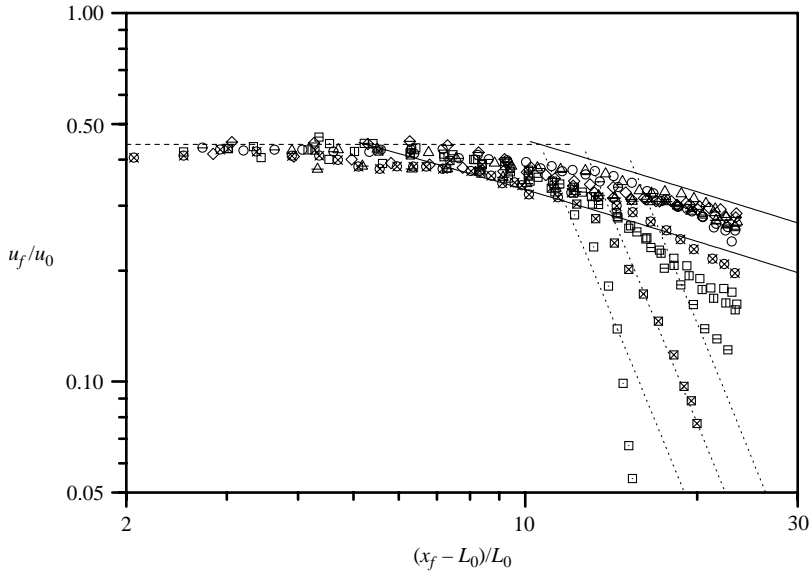


FIGURE 6. Evolution of the front velocity for the same full-depth releases ($\phi_0 = 1$) reported in figure 5. The lines indicate the corresponding power law behaviour for the three phases.

The time origin for the self-similar curves is determined by the theory, that is to say $x_f = 0$ for $t = 0$. On the other hand, the initial condition of the experiments ($x_f = L_0$ for $t = 0$) and the small time taken to withdraw the gate introduce a time origin shift of the order of t_c in the experimental data. However, any resulting error when laboratory results are compared with the asymptotic relationship becomes negligible for $t \gg t_c$.

The dotted lines in figure 5 are calculated using (2.7) and correspond to the viscous phase of three cases in which such a stage seems to be reached. The transition between stages is quite smooth, and only in some cases does the evolution of the front position pass through all three stages. The self-similar regime, if developed, may be very short. Particularly when small volumes are released (squares), the current may enter the viscous stage directly from the constant-velocity phase. Therefore, a determination of ξ based on the self-similar law in a position *vs.* time graph may be in error owing to an early presence of viscous effects.

As an alternative, we plot the front velocity $u_f = dx_f/dt$ as a function of the front position x_f as shown in figure 6. As expected, the experimental data follow the straight lines in a log-log graph corresponding to the three typical stages of a gravity current. The effects of the different values of the dimensionless constant ξ on the self-similar laws (2.3) are more evident in this plot. In addition, the dashed, solid and dotted lines show more abrupt changes in trends than in figure 5, partially because of the use of the front position as the abscissa instead of the time. Consequently, this representation provides a more sensitive test of the flow regimes.

4.1.2. Partial-depth releases

Figure 7 shows the images after processing and the equivalent height profiles for an experiment with $\phi_0 = 0.55$. Again the raised head and the instabilities and mixing at the top of the current are visible. In this case, the head is deeper and the following

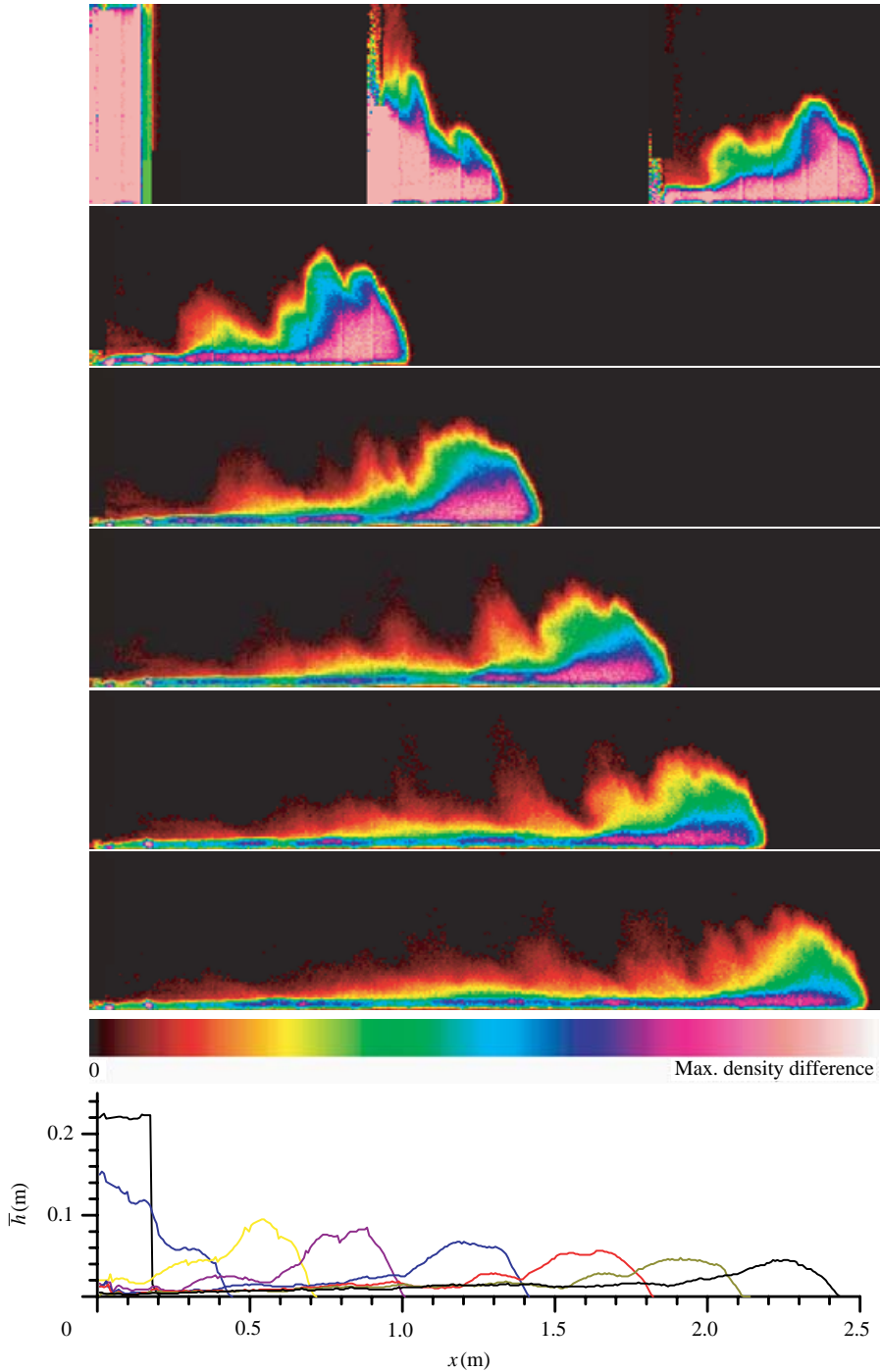


FIGURE 7. Images in false colour for fluid density and the corresponding equivalent depth profiles for a partial-depth release (run 17) with fractional depth $\phi_0 = 0.55$ (see table 1) for $t = 0, 1.71, 3.87, 6.03, 9.15, 12.51, 15.23$ and 18.47 s. The (expanded) vertical scale is the same for all the images; the first panel is higher because of the space occupied by the dense fluid initially.

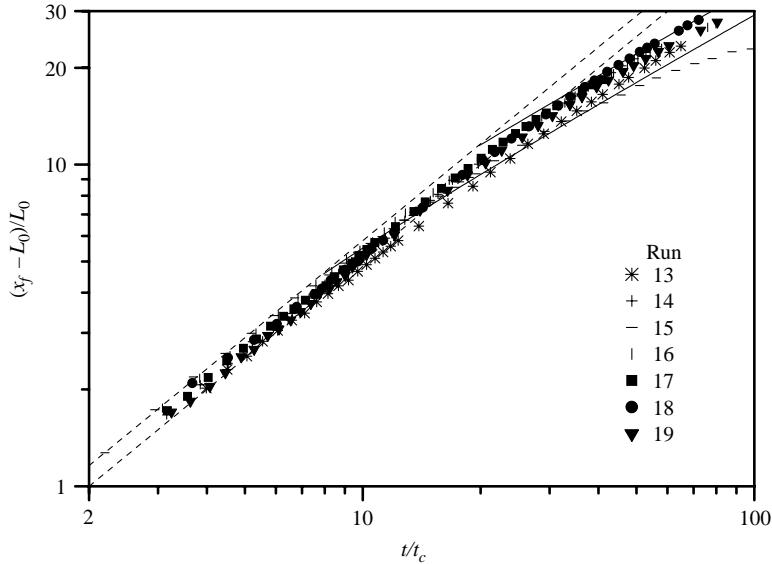


FIGURE 8. Dimensionless front position as a function of dimensionless time for partial-depth releases ($\phi_0 < 1$). The theoretical front evolution for the constant-velocity phase and the inertial self-similar regime are indicated by dashed and solid lines, respectively. The two curves in each case are chosen to bracket the data.

current is shallower than those corresponding to the full-depth release shown in figure 4. Nevertheless the length of head remains greater than its height.

The evolutions of the dimensionless front positions for runs 13–19, for which the initial fractional depth is $\phi_0 < 1$, are shown in figure 8. As for the full-depth releases, these currents also exhibit a constant-velocity phase initially. However, in this case the initial front velocity u_{f0} depends on the initial depth ratio ϕ_0 . The dashed lines corresponds to the limit straight lines with slope 1 that bracket the data. Also shown in figure 8 are the lines describing the theoretical similarity phase with values of $\xi = 1.4$ and 1.8 that span the data.

The graph of the dimensionless front velocity as a function of the dimensionless front position is shown in figure 9. Both the constant-velocity and the similarity regimes show variations which are associated with the different values of the initial fractional depth ϕ_0 , with higher dimensionless speeds u_f/u_0 occurring for lower values of ϕ_0 . This behaviour in the constant-velocity regime is consistent with the theories discussed in §2, and this trend persists into the similarity regime. (The outlier is run 15 which is influenced by viscous effects.)

Figure 10 shows the initial front velocity u_{f0} non-dimensionalized by u_0 in the constant-velocity phase for different initial depth ratios ϕ_0 . Also shown in the figure are experimental results reported by Rottman & Simpson (1983) and Shin *et al.* (2004). We see that the data are consistent, and they show a reduction in the Froude number based on the initial reduced gravity and depth of dense fluid. This reduction is consistent with the theoretical predictions of Shin *et al.* (2004). The consistency of these data show that the initial front speed is independent of the lock aspect ratio D/L_0 . For the present experiments $1 < D/L_0 < 4$, while for Rottman & Simpson (1983) $D/L_0 \leq 1$, and $D/L_0 \rightarrow 0$ in the experiments of Shin *et al.* (2004).

For $\phi_0 < 1$, the constant-velocity regime is maintained for a shorter distance than the 8–10 lock lengths found for $\phi_0 = 1$. Figure 11 shows the distance x_s that the

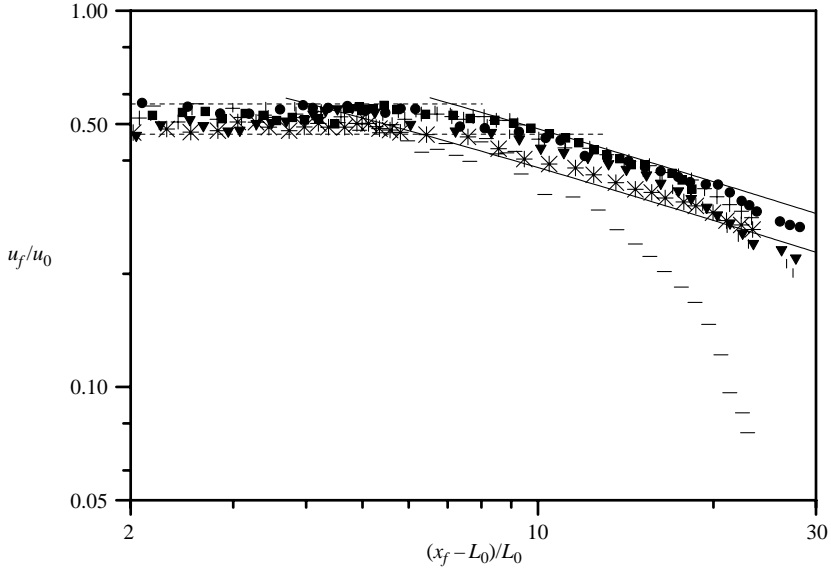


FIGURE 9. Evolution of dimensionless front velocity for $\phi_0 < 1$. The theoretical estimates for the constant-velocity phases and the self-similar regimes are indicated by the dashed and solid lines, respectively.

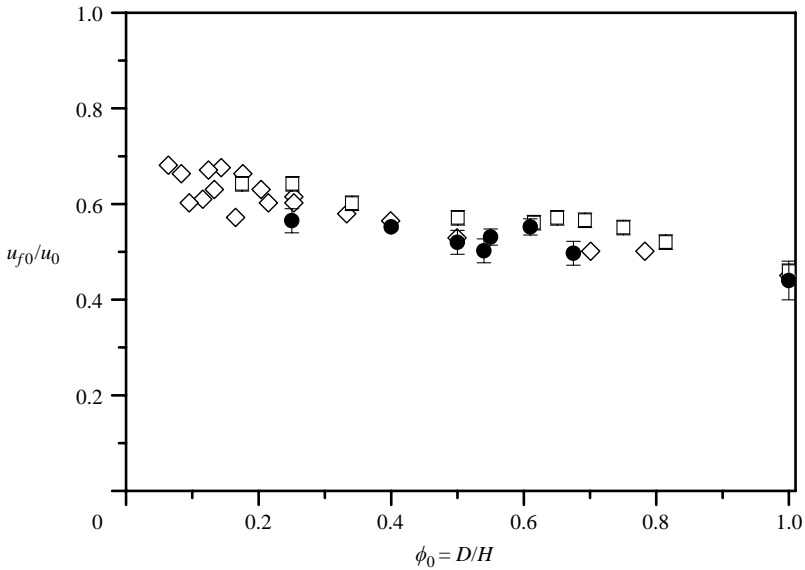


FIGURE 10. The dimensionless front speed during the constant-velocity regime as a function of the initial aspect ratio ϕ_0 (●). For comparison, data by Rottman & Simpson (1983) (◊) and Shin *et al.* (2004) (□) are also shown.

front travels before leaving this initial regime as a function of ϕ_0 (solid squares). The open symbols correspond to the averaged values of the case $\phi_0 = 1$; runs 1–3 have been plotted separately (open circles) since the similarity phase seems to be absent in these runs as observed in figures 5 and 6. Also included in figure 11 is the transition length determined experimentally by Rottman & Simpson (1983) (solid

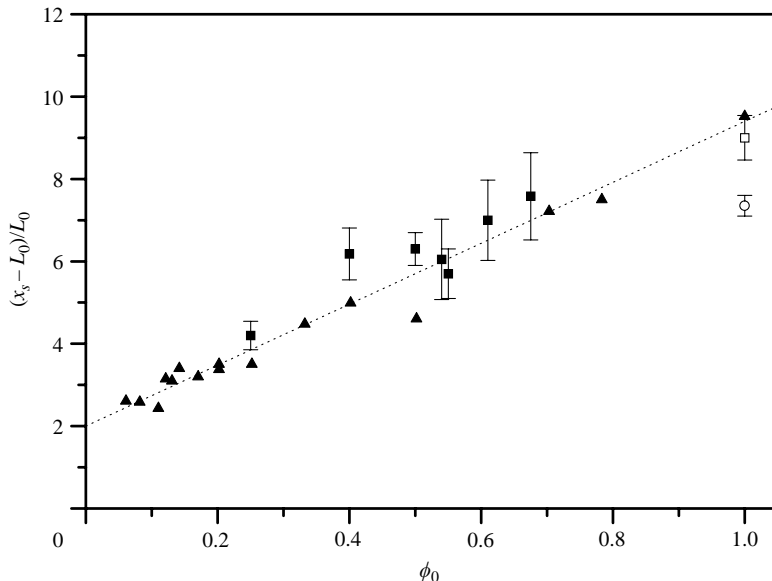


FIGURE 11. Length in units of L_0 at which the front evolution departs from the constant-velocity phase as a function of the initial fractional depth ϕ_0 . The present data for $\phi_0 < 1$ are shown as ■, while for $\phi_0 = 1$ the results are averaged to give □ for runs 4–12 and ○ for runs 1–3. The results obtained by Rottman & Simpson (1983) (▲) and the relation cited by Hallworth *et al.* (1996) (dashed line) are also shown.

triangles) and the empirical law based on those results given by Hallworth *et al.* (1996), $x_s/L_0 = 3 + 7.4\phi_0$. Except for runs 1–3, our experiments agree well with these previously reported results.

4.2. Current height profiles

4.2.1. Full-depth releases

A time series of profiles for a full-depth release is shown in figure 12. The current rapidly develops an elevated head which contains most of the fluid from the lock. This rapid development of the head is associated with the large aspect ratio $D/L_0 = 2$ of the lock, and has been previously observed by Hacker, Linden & Dalziel (1996). The depth of the head stays roughly constant until the current has propagated about 10 lock lengths, and then it begins to decrease. In this initial phase, the depth of the current behind the head stays roughly constant for about 10 head heights back from the front and then it decreases towards the rear. At later times the depth decreases more gradually towards the rear and extends further back from the front. These properties are also observed in the images shown in figure 4.

This transition from a state in which most of the dense fluid is contained in a single ‘head-like’ region to another characterized by a distinct head with a significant ‘tail’ seems to be associated with the fluid left behind as the front propagates. Perturbations are successively generated at the current front and propagate forwards, but at a speed significantly less than the front speed itself. In fact in the later stages, these waves are almost stationary in the laboratory frame. We analyse these profiles by looking, in turn, at the constant-velocity, similarity and viscous phases of the current.

Figure 13(a) shows equivalent height profiles for a full-depth release during the constant-velocity phase for different times. In figure 13(b), these profiles are scaled by

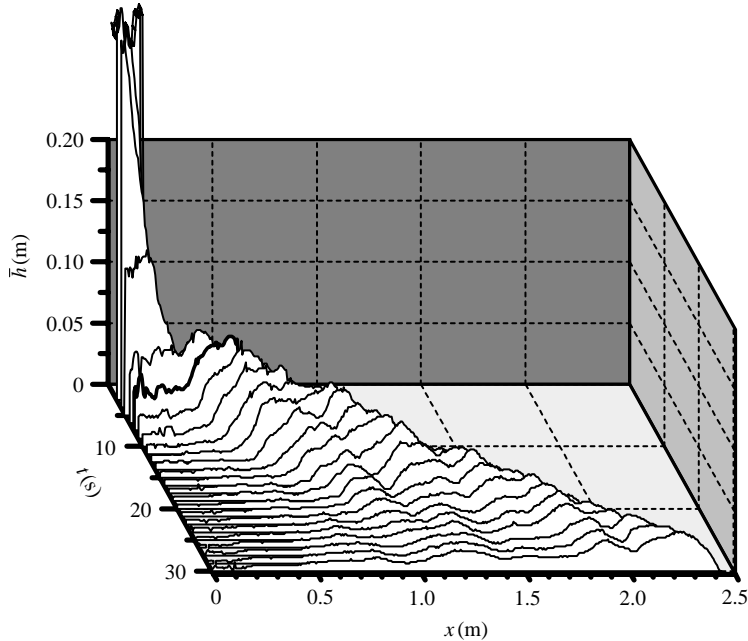


FIGURE 12. A time sequence of equivalent height profiles for a full-depth release $\phi_0 = 1$. The case shown is run 10.

the front position x_f . Initially the depth of the current is approximately constant along its length. Although as reported above, the speeds of these currents are consistent with the energy conserving theories of Benjamin (1968) and Shin *et al.* (2004), the depths of the current, are below the half-depth required by these theories. Shin *et al.* (2004) show that the depths of the currents are altered by different initial conditions in lock release, and this may be the result of the lock aspect ratios in the present experiments being large ($D/L_0 = 1-4$). As the ambient fluid enters the lock, the depth of the dense fluid in the lock decreases and a reflected disturbance propagates forwards out of the lock towards the head. In front of this disturbance, the height of the current remains constant. As the disturbance catches up with the front, an elevated ‘head’ region is formed between the front and the disturbance, as can be seen in figure 13(b). Eventually the disturbance reaches the front and the similarity phase occurs as noted previously by Rottman & Simpson (1983).

After the onset of the similarity phase, the length of the head remains approximately constant. Equivalent height profiles for the similarity phase are shown in figure 14. In this figure, the length of the current has been normalized by the distance x_r from the lock to the rear of the head and the depth has been normalized by the depth \bar{h}_r at that location. The collapse of the profiles at different times shows that during this phase the shape of the current behind the head is, indeed, self-similar, as predicted by Rottman & Simpson (1983) and Gratton & Vigo (1994).

Figure 14 also shows similarity solutions (2.4) of the shallow-water equations, for three different values of the front Froude number $F_f = 1.4, 1.6$ and 1.8 . Qualitatively, the current has the same form as these theoretical profiles, with the current becoming deeper towards the front. It appears that the solution with $F_f = 1.8$ gives the best fit to the experimental profiles.

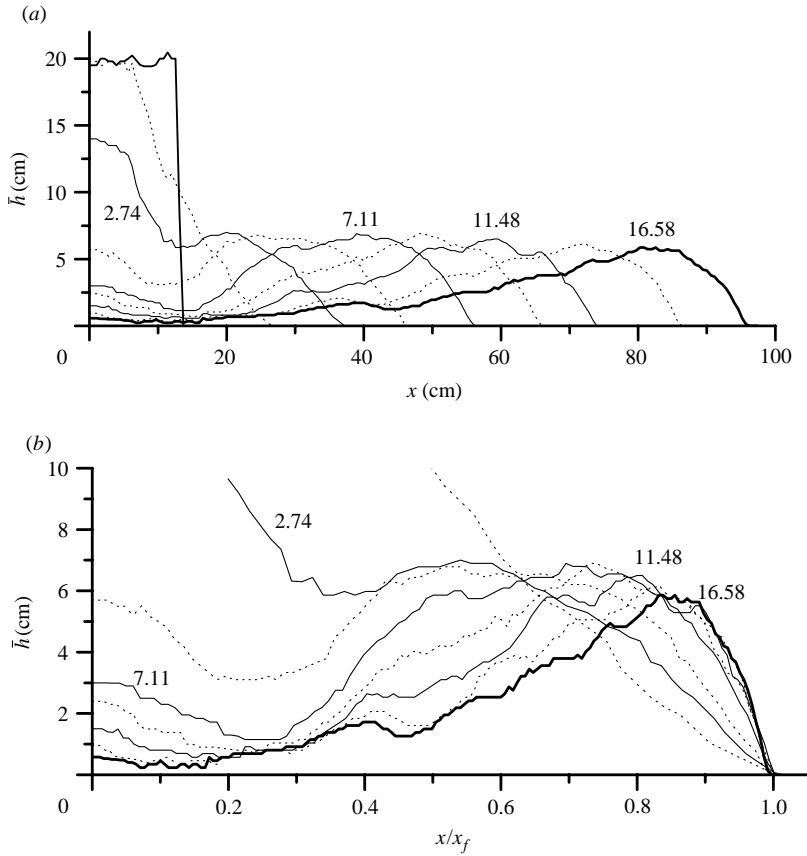


FIGURE 13. (a) Equivalent height profiles of a gravity current with $\phi_0 = 1$ (run 6) at $t/t_c = 0, 1.29, 2.74, 4.93, 7.11, 9.30, 11.48, 13.66$ and 16.58 . (b) The same profiles shown in (a) but with the abscissa scaled with x_f . Times are indicated for profiles represented by solid lines, and intermediate profiles are plotted with dotted lines.

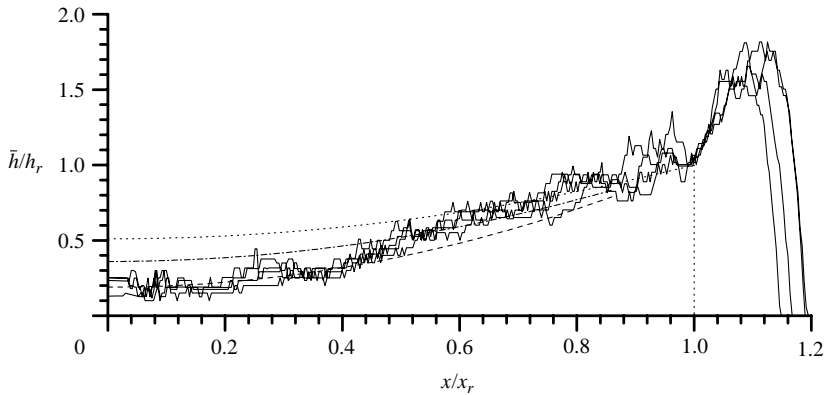


FIGURE 14. Equivalent height profiles for a full-depth release $\phi_0 = 1$ (run 8) in the similarity phase with $t/t_c = 43.4, 46.9, 49.8$ and 56.8 . The depth is scaled with \bar{h}_r and the length with the distance to the rear of the head x_r . The profiles depicted by dotted, dash-dotted and dashed lines correspond to (2.4) for $F_f = 1.4, 1.6$ and 1.8 , respectively. In order to be consistent with the similarity theory, x_f is replaced by the distance to the rear of the head x_r .

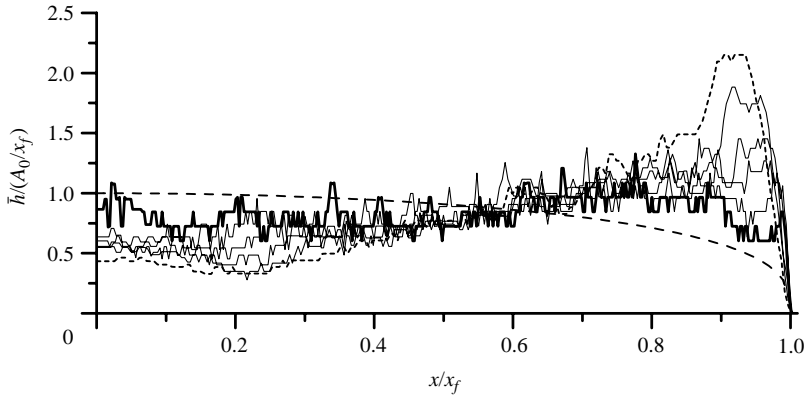


FIGURE 15. Dimensionless equivalent height profiles for run 4 ($\phi_0 = 1$) as the current enters the viscous phase. The profiles are shown at $t/t_c = 20.2$ (thick dotted line), 28.4, 35.9, 43.4, 57.8 and 76.2 (thick solid line). The profile depicted by a dashed line corresponds to the asymptotic viscous regime (2.9).

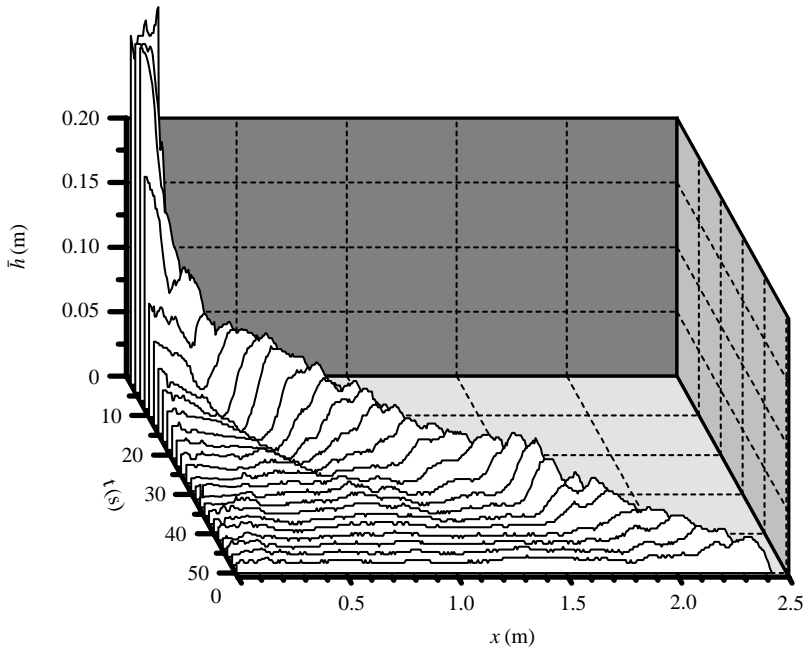


FIGURE 16. A time sequence of equivalent height profiles for $\phi_0 = 0.675$ (run 13).

The equivalent height profiles for a gravity current entering the viscous regime are shown in figure 15. The depth is scaled with A_0/x_f and the length with the distance x_f to the front. Note that the height of the head decreases with time and eventually disappears, and the current shape tends to the theoretical viscous profile (2.9) indicated by the dashed line.

4.2.2. Partial-depth releases

Similar profiles to those shown in §4.2.1 were also obtained for the partial-depth releases. A time sequence of current height profiles for run 13 with $\phi_0 = 0.675$ is shown in figure 16. Comparison with the full-depth release of figure 12, shows that

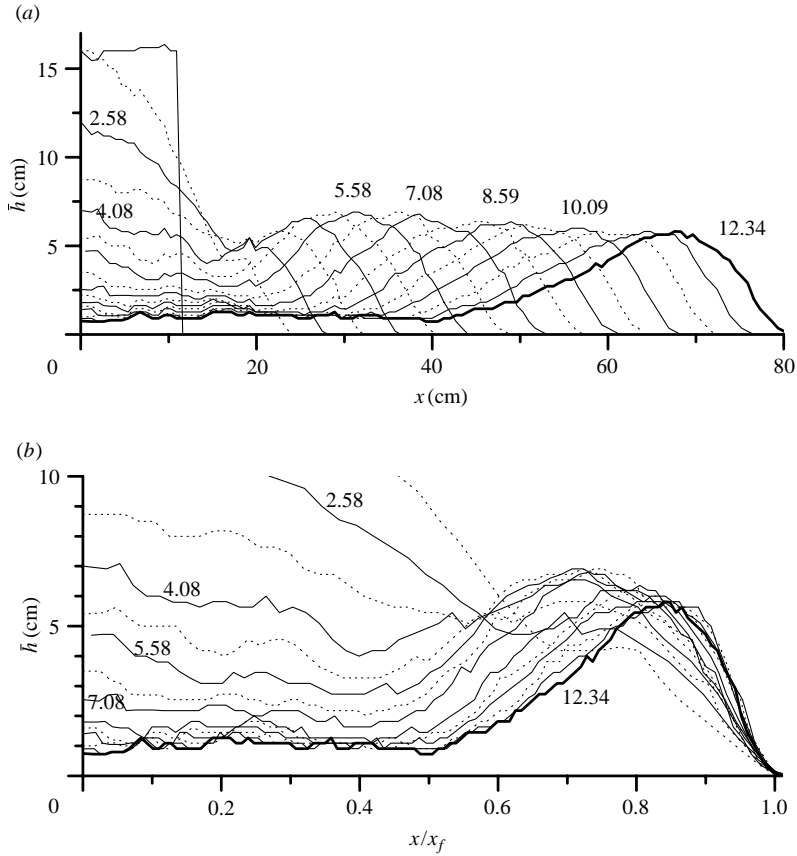


FIGURE 17. (a) Equivalent height profiles for a partial-depth release with $\phi_0 = 0.4$ (run 16) in the constant-velocity phase at $t/t_c = 0, 1.83, 2.58, 3.33, 4.08, 4.83, 5.58, 6.33, 7.08, 7.83, 8.59, 9.34, 10.09, 10.84, 11.59$ and 12.34 . (b) The same profiles with horizontal positions scaled with x_f . Times are indicated for profiles represented by solid lines, and intermediate profiles are plotted with dotted lines.

the current volume is concentrated more towards the front and the perturbations are less pronounced. The current depth behind the head is more uniform than in the full-depth case, and the fluid depth in the lock does not decrease as much as for $\phi_0 = 1$. These results are also consistent with the observations of Rottman & Simpson (1983), who showed that the reflected disturbance from the lock was a bore for large fractional depths, but took the form of an expansion wave at lower fractional depths.

Profiles for run 16 with $\phi_0 = 0.4$ are shown in figure 17. Comparison with the equivalent full-depth releases in figure 13 confirms the observations mentioned in the previous paragraph. As for $\phi_0 = 1$, we observe that the head height remains constant while the depth of the following flow decreases with time. It is clear that in both these cases the fluid volume in the ‘head’ remains approximately constant or decreases slowly with time, so that the head is not being supplied from the rear by the following current. This constancy, despite the observed mixing, is a result of the fact that determining the depth of the current by integrating the density captures all the dense fluid even when it is mixed with the ambient fluid.

The similarity phase and the approach to the viscous phase for a partial-depth release are shown in figures 18 and 19, respectively. As for the full-depth releases,

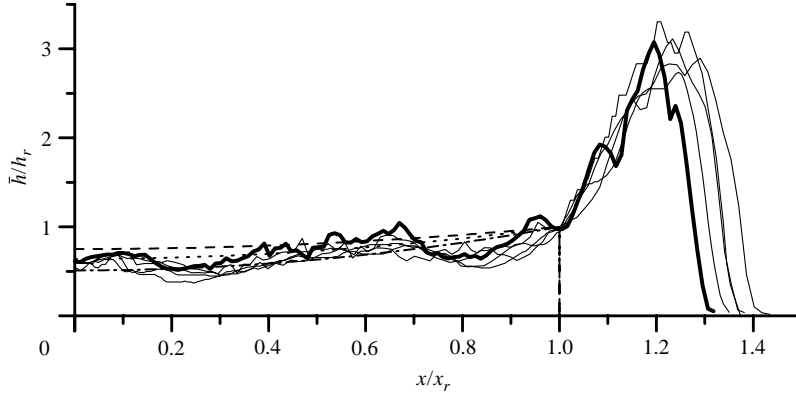


FIGURE 18. Profiles for a partial-depth release (run 16) in the similarity phase with $t/t_c = 21.35, 23.60, 25.86, 28.11$ and 31.11 (thick solid line). The profiles depicted by dotted, dash-dotted and dashed lines correspond to similarity solutions to the shallow-water equations with $F_f = 1.0, 1.2$ and 1.4 , respectively.

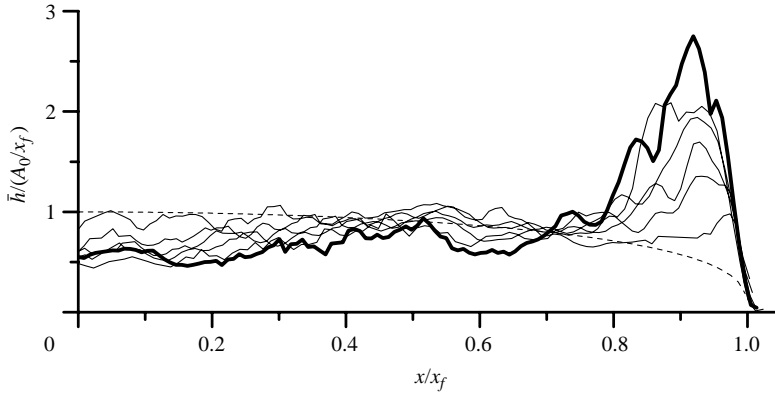


FIGURE 19. Equivalent height profiles of the gravity current shown in figure 18 as it enters the viscous phase. The profiles are shown at $t/t_c = 31.11, 36.40, 43.15, 49.91, 57.42$ and 79.20 . The profile depicted by a dashed line corresponds to the asymptotic viscous regime (2.9).

the profiles for the currents are self-similar in the similarity phase. After $t/t_c = 31.11$, shown as the thick solid profile in both figures, the head begins to decrease and the current approaches the viscous phase, and ultimately a good agreement with the corresponding theoretical profile is observed.

4.3. Froude numbers

During the constant-velocity phase (figures 13 and 17) the gravity current is characterized by an almost constant depth from the head to the point reached by the reflected disturbance from the lock. This allows a current depth to be defined ahead of this disturbance which can be used to determine the Froude number of the current (Shin *et al.* 2004). However, once the current enters the similarity phase, there is a distinct difference between the height of the head and the depth of the current in the following flow. This variation in the current profile makes it difficult to decide the characteristic height for determining the Froude number. Consequently, we calculate the Froude number using depths at different locations in the flow.

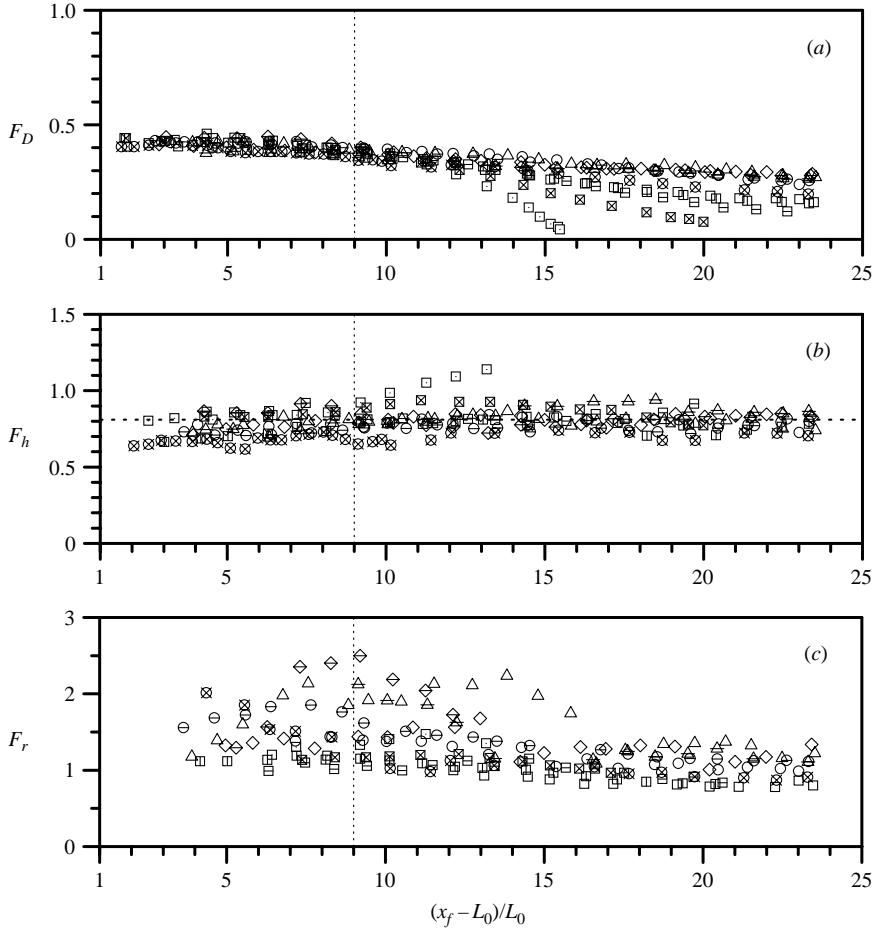


FIGURE 20. Evolution of the Froude number for the full-depth releases ($\phi_0 = 1$) considering (a) the initial height of dense fluid, (b) the maximum equivalent height and (c) the equivalent height just behind the head. The vertical dashed line indicates approximately the departure from the constant-velocity phase. The horizontal line in (b) is the average value obtained in the similarity regime.

The Froude number, based on the front velocity u_f , and three different depths – the lock depth D , the maximum height of the head \bar{h}_m and the height at the rear of the head \bar{h}_r – is plotted in figure 20 for the full-depth releases $\phi_0 = 1$. In each case, the lock buoyancy g'_0 is used to estimate the corresponding Froude number.

The Froude number F_D (figure 20a) based on the initial lock depth is approximately constant during the constant-velocity phase ($x \leq 10L_0$) as expected. The value $F_D = 0.45$ for the initial phase is consistent with previous measurements (see Shin *et al.* 2004). After about 10 lock-lengths the similarity phase begins, and the value of F_D decreases.

Figure 20(b) shows the Froude number based on the maximum height of the head

$$F_h = u_f / \sqrt{g'_0 \bar{h}_m}. \quad (4.1)$$

During the constant-velocity phase, F_h exhibits some scatter but this scatter is reduced in the similarity phase. In particular, for $x_f \geq 10L_0$, F_h is approximately constant with

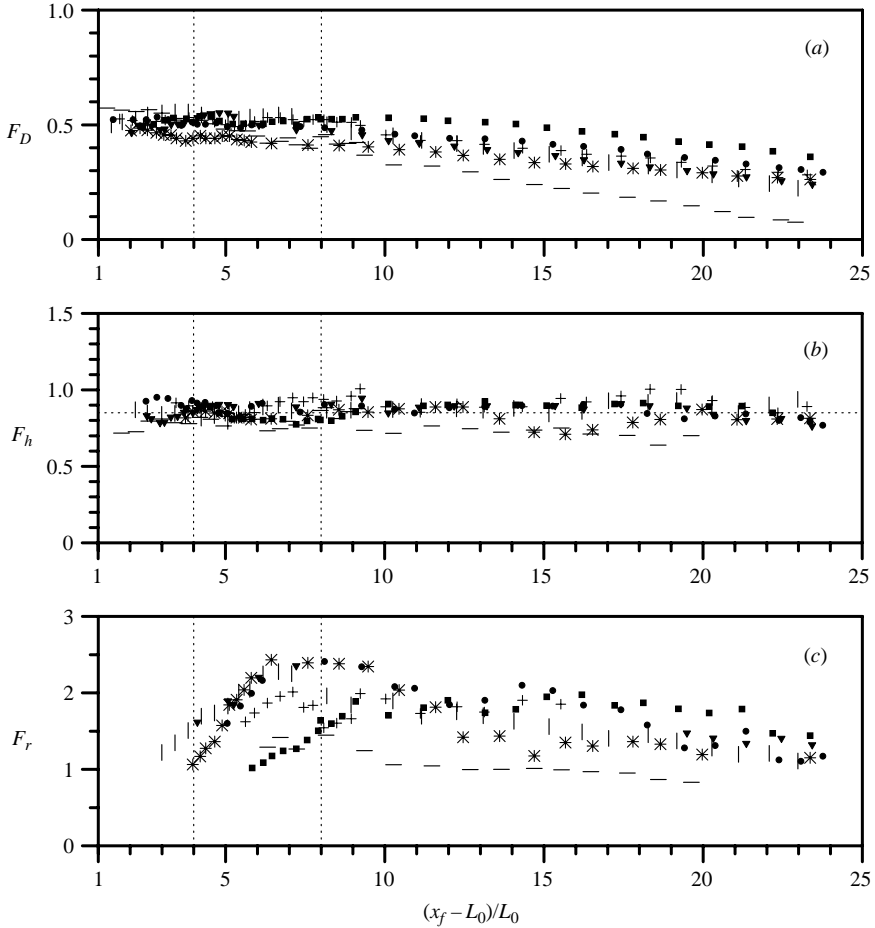


FIGURE 21. Evolution of the Froude number for the partial-depth releases ($\phi_0 < 1$) considering (a) the initial height of dense fluid, (b) the maximum equivalent height and (c) the equivalent height just behind the head. The vertical dashed lines indicate the departure from the constant-velocity phase, observed to be later for larger ϕ_0 . The horizontal line in (b) is the average value obtained in the similarity regime.

a mean value $\langle F_h \rangle = 0.81 \pm 0.10$. This measure of the Froude number collapses the data at large x_f , in contrast with F_D , which only applies for the constant-velocity phase. (The outliers are runs 1–3, which have also shown a different behaviour in their front evolution (figures 5 and 6) because they have the lowest Reynolds numbers – see table 1.)

The Froude number F_r , based on the buoyancy at the rear of the head, plotted in figure 20(c), shows considerable variation among experiments and tends to decrease with the distance from the lock.

The Froude numbers F_D , F_h and F_r for the partial-depth releases $\phi_0 < 1$ are shown in figure 21. In this case, since u_{f0} is a function of ϕ_0 (see figure 10), F_D has higher values and a greater variability in the velocity-constant phase. However, as we discussed in relation to figure 10, this variation is consistent with previous measurements.

In the similarity phase, the Froude number based on the maximum height of the head again collapses the data on an approximately constant value whose average

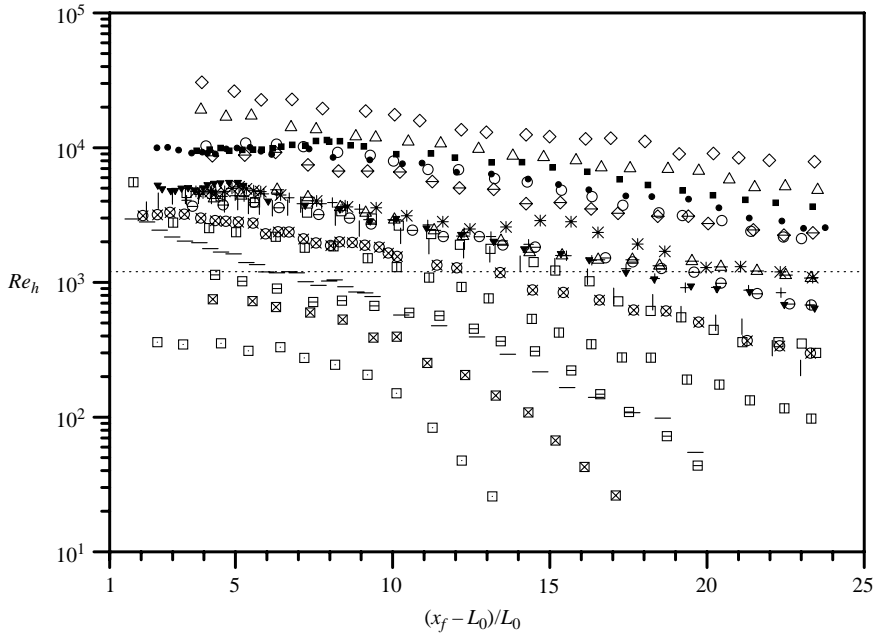


FIGURE 22. Evolution of the Reynolds number based on the equivalent height of the head.

value is $\langle F_h \rangle = 0.86 \pm 0.10$ (dotted horizontal line in figure 21b). (The outlier is run 15 which also shows a different behaviour in the front evolution, figures 8 and 9, as a result of its low Reynolds number.) The Froude number F_r based on the buoyancy at the rear of the head (figure 21c) again shows considerable variation among experiments as in the full-depth releases plotted in figure 20(c).

Finally, figure 22 shows the Reynolds number $Re_h = \bar{h}_m u_f / \nu$, based on the equivalent height of the head and the front velocity, as a function of the distance along the channel. The experimental data for runs 1 and 15, for which F_h departs from the general trend in the similarity regime in figures 20(b) and 21(b), and also are cases where x_f and u_f are not consistent with the self-similar law in figures 5, 6, 8 and 9, are associated with Reynolds numbers $Re \leq 1200$ (dotted line in figure 22), suggesting that viscous effects are important in these cases (Simpson 1997). In addition, runs 3–5, 7, 16 and 19 require a more careful analysis because they have only a short stage in which the front evolution follows the expected similarity power law since the Reynolds number decreases below 1200. We discuss these special cases in § 5.

5. Discussion

Figure 23 presents the Froude number F_h based on the maximum head height in the similarity phase shown in figures 20(b) and 21(b) as a function of the fractional depth $\phi_h = \bar{h}_m / H$ based on the instantaneous head height. The data show some scatter, but appear to approach a limiting value of F_h for $\phi_h \rightarrow 0$. In particular, for $\phi_h < 0.15$, the average of all values gives $\langle F_h \rangle = 0.86 \pm 0.10$, and this value is taken as the limit for small fractional depths. At larger values of $\phi_h > 0.2$ there is a decrease in F_h with increasing ϕ_h .

In this figure we also show the curve representing the relationship (2.13) from Shin *et al.* (2004) for the Froude number as a function of the initial fractional depth in the constant-velocity phase. The experimental data lie below this curve in the whole

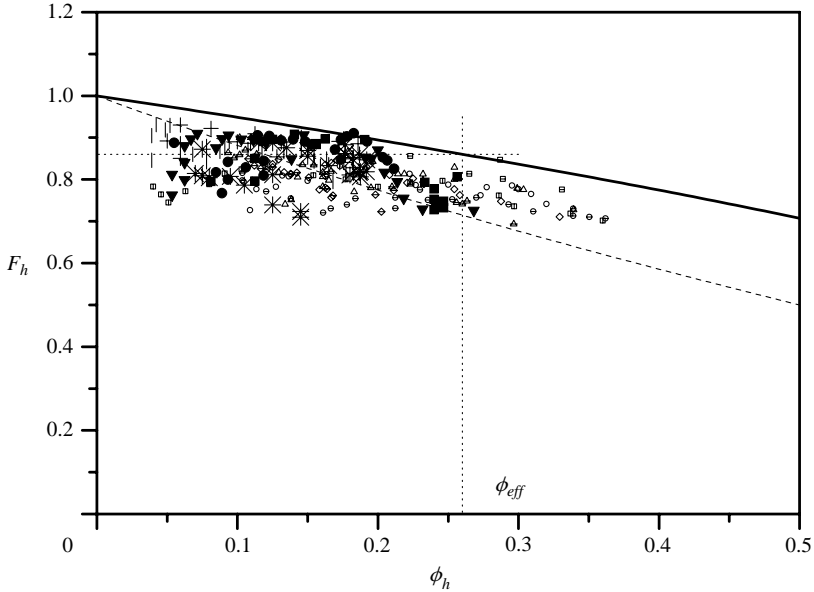


FIGURE 23. Froude number at the front as a function of the instantaneous fractional depth for the similarity phase. The solid line is given by (2.13) and the dashed line by (2.12) with the empirical coefficient $\beta^2 = 1$. The value $F_h(\phi_h \rightarrow 0) = 0.86$ (horizontal dotted line) and the solid line given suggest $\phi_{eff} \approx 0.26$.

range of ϕ_h obtained. This difference may result from the depth used in (2.14) being the depth in the hydrostatic part of the flow, not at the head where non-hydrostatic processes are significant. The Rottman & Simpson (1983) formulation of the Benjamin front condition with the parameter $\beta^2 = 1$ obtained by fitting their experimental data is also shown in figure 23. This formula passes through the data points, but the dependence on ϕ_h is larger than observed, especially for small ϕ_h .

The two-layer theories of Benjamin (1968) and Shin *et al.* (2004) assume that there is no stress at the lower boundary and that the velocities in the two layers are constant with height. When the ambient fluid is much deeper than the current, this latter approximation is not strictly correct. There will be flow in the ambient close to the current, but the velocity will decrease with distance above the current.

The effect of the velocity distribution in the ambient fluid can be modelled as follows. Suppose that only a part $z < H_{eff}$ of the ambient fluid participates in the hydrodynamic drag on the current. It seems reasonable to suppose that, in the rest frame of the current, the velocity of the ambient fluid changes from $u \approx u_1$ for $z < H_{eff}$ to $u \approx u_f$ for $z > H_{eff}$ with a smooth transition at $z \approx H_{eff}$, as indicated by the arrows in the idealized sketch depicted in figure 24. Dimensional analysis suggests that the thickness of the ambient fluid layer involved in the form drag should be of the order of the gravity current depth when the ambient fluid depth H is too large to be a characteristic depth of the flow related to the dense current.

An estimate of H_{eff} may be obtained by considering $u = u_1$ for $z \leq H_{eff}$, and ignoring the fluid above $z > H_{eff}$ in the local momentum balance in the front region (i.e. taking $u = u_f$ for $z > H_{eff}$). Replacing F and ϕ with the values of the $F_h(\phi \rightarrow 0)$ and $\phi_{eff} = \bar{h}_m / H_{eff}$, respectively, (2.13) becomes

$$\phi_{eff} = [1 - F_h^2(\phi_h \rightarrow 0)]. \quad (5.1)$$

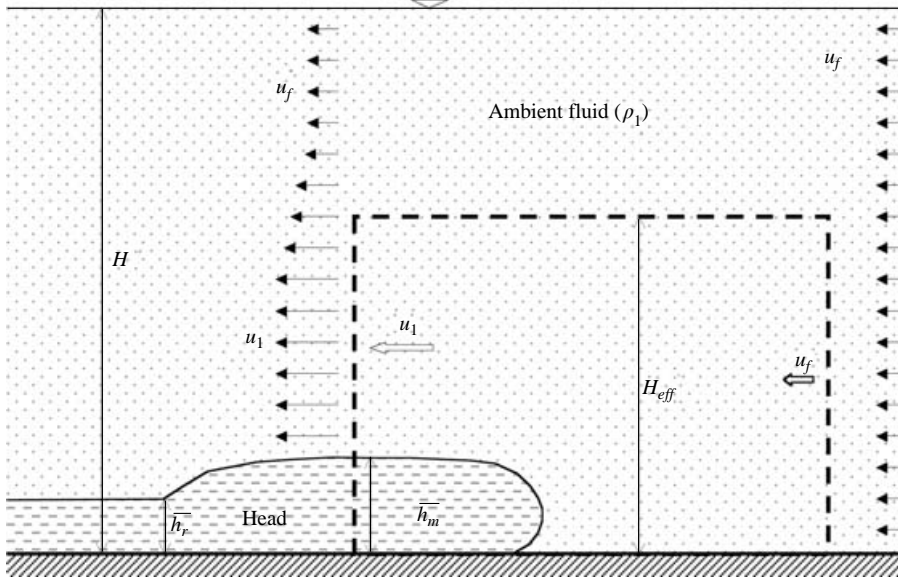


FIGURE 24. Flow around the gravity current for a deep ambient fluid in the frame of reference moving with the head.

Thus the suggested experimental value $F_h(\phi \rightarrow 0) \approx 0.86$ provides an estimate of $\phi_{eff} \approx 0.26$ and then $H_{eff} \approx \bar{h}_m / 0.26 \approx 3.85\bar{h}_m$. According to this estimate, the depth of the ambient fluid layer involved in the drag is about four times the depth of the gravity current head, in agreement with the above dimensional considerations.

This value of $\phi_{eff} \approx 0.26$ is shown in figure 23. For smaller values of ϕ_h the front Froude number F_h is approximately constant, while for larger values F_h decreases, in a manner consistent with (2.13). This behaviour supports the idea that a local momentum balance applies at the head during the similarity phase.

While the Froude number based on the local head height is constant during the similarity phase, the value for a deep ambient fluid, $F_h(\phi_h \rightarrow 0) \approx 0.86$, implies that the similarity coefficient in (2.6) is $\xi \approx 1.24$. This value is small when it is compared with those obtained from figures 5, 6, 8 and 9. Consequently, the self-similar flow described in §2.1 seems to be connected with the depth of the current behind the head, and not with the head height in a direct way.

In the similarity phase, (2.6) shows that ξ is an increasing function of the front Froude number F_f . Figure 25 shows values of ξ , determined from the front positions, plotted as functions of F_h and F_r . The value of ξ is not uniquely related to the Froude number F_h , but increases with the Froude number F_f taken as the Froude number F_r based on the height \bar{h}_r at the rear of the head. This trend is consistent with (2.6), but the dependence is not as strong as the theory suggests. The error bars for F_r are mainly determined by the uncertainty in the measurements of h_r resulting from variations in depth owing to flow perturbations such as those shown in figure 12.

While the variations in the value of ξ are correlated with the Froude number F_r based on the depth at the rear of the head, we also find the values vary with the Reynolds number of the head. This relationship is shown in figure 26 which shows that ξ increases with Reynolds number. This correlation implies that F_r increases with Reynolds number, while F_h remains constant.

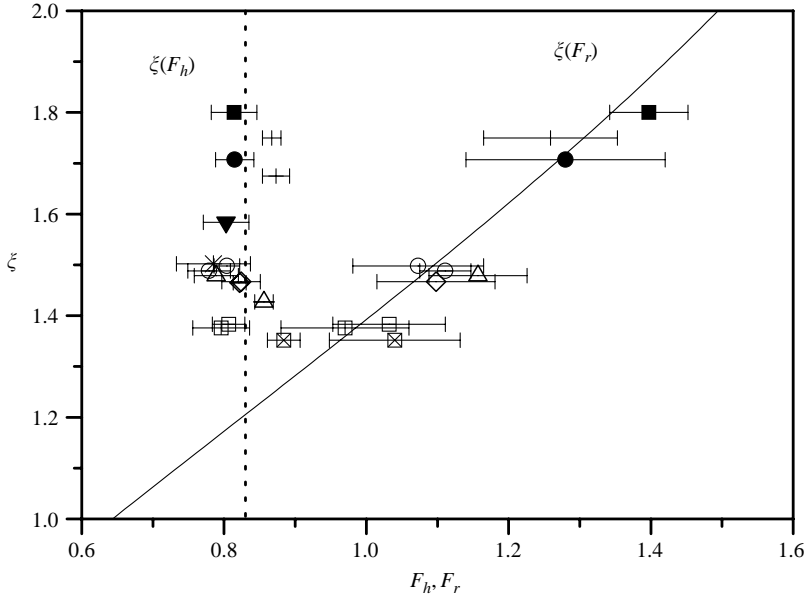


FIGURE 25. Coefficient ξ of the self-similar law for the front position evolution as a function of the Froude number calculated with \bar{h}_m and \bar{h}_r . (Symbols are associated with runs indicated in table 1.)

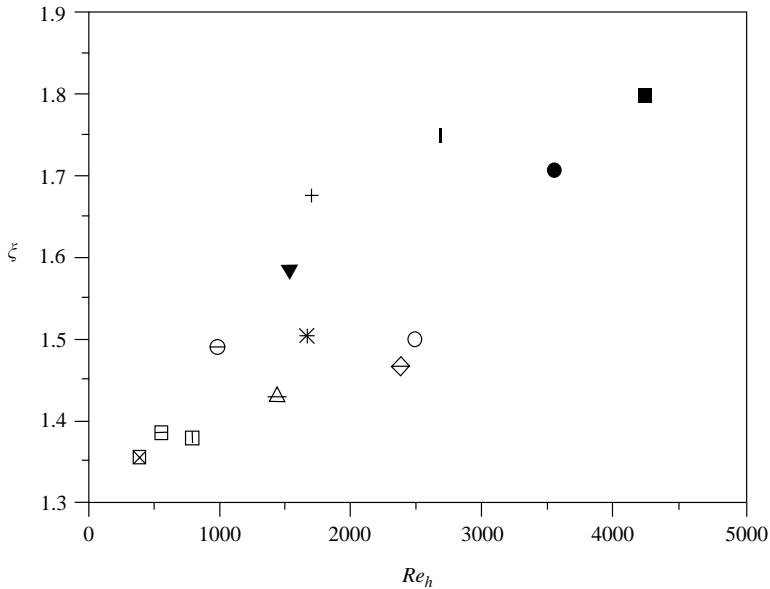


FIGURE 26. Coefficient ξ of the self-similar law as a function of the Reynolds number calculated with \bar{h}_m .

Figures 25 and 26 include the values of ξ for runs 3–5 which have only a short similarity phase before the currents enter the viscous regimes and for these cases $400 < Re_h < 1000$. The corresponding data points are consistent with the rest of the results. For runs 7, 16 and 19 this phase is also short, but the corresponding Re

is higher ($Re \gtrsim 1000$). Figure 26 suggests that the lower limit $\xi \approx 1.24$ cited above corresponds to currents with low Reynolds numbers, and which may be entering the viscous phase.

Unfortunately, our results do not allow us to infer whether ξ and F_r have asymptotic values for large Reynolds numbers or not. If these asymptotic values exist, the corresponding experiments seem to be out of the range of our experiments. Studies at higher Reynolds numbers are needed to elucidate this point.

6. Conclusions

We have presented the first objective measurements of the shape and buoyancy of a gravity current during its successive phases when it is generated by a lock release. As a consequence, we have been able to measure the Froude number of the currents as they evolve in space and time.

It is well established that when dense fluid is released from a lock, the motion of the ensuing current has three phases. In the initial constant-velocity phase, the speed of the front is constant and the depth of the current increases from the front to a constant value. The Froude number F_D based on the initial lock depth D is constant during this phase and can be derived from energy-conserving theory (Shin *et al.* 2004).

This constant-velocity phase persists until the finite volume of the lock becomes significant. This transition occurs when a disturbance (either a bore or an expansion wave depending on the lock geometry) reflects from the back wall of the lock and catches up with the front. From that point, the current tends to a self-similar profile, in which the current depth increases towards the rear of the head. The head itself retains an almost constant height, and has an abrupt reduction in depth at its rear.

In the similarity phase, the current shape behind the head is consistent with a similarity solution of the shallow-water equations, with the current depth increasing towards the head. A remarkable feature of the current during this phase is that the Froude number F_h based on the maximum height of the head is approximately constant with a value of 0.86. Thus the current undergoes a transition from an initial regime when the Froude number based on the initial conditions (the lock depth) is constant to one in which the current head is in a local balance.

The constancy of the Froude number F_h based on the head height in a deep ambient fluid is consistent with a local momentum balance in the similarity phase. In this case, our measurements suggest that the effect of the current on the ambient fluid extends to about four times the height of the head. Above that height the ambient fluid is unaffected by the current.

Finally, there is a viscous phase in which the buoyancy forces are balanced by viscous drag. Our experiments show that the head decreases in height and eventually disappears and that the profiles are consistent with lubrication theory (Huppert 1982).

We now return to a major issue of the application of gravity current theory to practical situations. These often involve similarity solutions of the shallow-water equations and solutions to simpler integral models where the shape and structure of the current is assumed *a priori*. Both approaches require the specification of a front condition, and this usually takes the form of the specification of the front Froude number as a function of the fractional depth. Since there is an inertial-buoyancy balance in both the constant-velocity and similarity phases, the Froude number for the constant-velocity phase (both theoretical, e.g. Benjamin 1968; or experimental, e.g. Huppert and Simpson 1980) has been applied. However, there is no justification for this assumption.

On the contrary, our results suggest that using only a front Froude number based on the head height is, strictly speaking, not appropriate for applications to similarity theories for the shallow-water equations. As shown in figure 25, the similarity coefficient ξ correlates with the Froude number F_r based on the buoyancy at the rear of the head. Unfortunately, F_r is not a constant and thus the ratio between both Froude numbers has to be related with an additional characteristic parameter of the flow, such as the Reynolds number (see figure 26). More work is required to obtain the relationship that relates both Froude numbers and the characteristic parameters of the flow.

This work was supported by CONICET, Argentina, under Grant PIP 2826 and by the US National Science Foundation under Grant CTS-0209194.

REFERENCES

- BARENBLATT, G. I. 1996 *Scaling, Self-Similarity and Intermediate Asymptotics*. Cambridge University Press.
- BARR, D. I. H. 1967 Densimetric exchange flows in rectangular channels. *La Houille Blanche* **22**, 619–631.
- BENJAMIN, T. B. 1968 Gravity currents and related phenomena. *J. Fluid Mech.* **31**, 209–248.
- DALZIEL, S. B. 1993 Rayleigh–Taylor instability: experiments with image analysis. *Dyn. Atmos. Oceans* **20**, 127–153.
- DALZIEL, S. B. 1995 *DigImage: System Overview*. Cambridge Environmental Research Consultants, UK.
- FANNELOP, T. K. & WALDMAN, G. D. 1972 Dynamics of oil slicks. *AIAA J.* **10**, 506–510.
- FAY, J. A. 1969 The spread of oils slicks on a calm sea. In *Oil on the Sea* (ed. D. P. Hoult), pp. 53–63. Plenum.
- GRATTON, J. & VIGO, C. 1994 Self-similar gravity currents with variable inflow revisited: plane currents. *J. Fluid Mech.* **258**, 77–104.
- GRUNDY, R. E. & ROTTMAN, J. W. 1985 The approach to the self-similarity of the solutions of the shallow-water equations representing gravity current releases. *J. Fluid Mech.* **156**, 39–53.
- HACKER, J., LINDEN, P. F. & DALZIEL, S. B. 1996 Mixing in lock-release gravity currents. *Dyn. Atmos. Oceans* **24**, 183–195.
- HALLWORTH, M. A., HUPPERT, H. E., PHILIPS, J. C. & SPARKS, S. J. 1996 Entrainment into two-dimensional and axisymmetric turbulent gravity currents. *J. Fluid Mech.* **308**, 289–311.
- HOULT, D. P. 1972 Oil spreading on the sea. *Annu. Rev. Fluid Mech.* **4**, 341–368.
- HUPPERT, H. E. 1982 The propagation of two-dimensional and axisymmetric viscous gravity currents over a rigid horizontal surface. *J. Fluid Mech.* **121**, 43–58.
- HUPPERT, H. E. & SIMPSON, J. E. 1980 The slumping of gravity currents. *J. Fluid Mech.* **99**, 785–799.
- KEULEGAN, G. H. 1958 The motion of saline fronts in still water. *Natl Bur. Stand. Rep.* 5813.
- LANDAU, L. D. & LIFSHITZ, E. M. 1987 *Course of Theoretical Physics, Volume 6: Fluid Mechanics*, 2nd edn. Pergamon.
- MARINO, B. M., THOMAS, L. P., DIEZ, J. A. & GRATTON, R. 1996 Capillary effects on viscous gravity spreading of wetting liquids. *J. Colloid Interface Sci.* **177**, 14–30.
- ROTTMAN, J. W. & SIMPSON, J. E. 1983 Gravity currents produced by instantaneous releases of a heavy fluid in a rectangular channel. *J. Fluid Mech.* **135**, 95–110.
- SHIN, J. O., DALZIEL, S. B. & LINDEN, P. F. 2004 Gravity currents produced by lock exchange. *J. Fluid Mech.* **521**, 1–34.
- SIMPSON, J. E. 1997 *Gravity Currents: In the Environment and the Laboratory*. Cambridge University Press, 258 pp.